Available online at www.sciencedirect.com
ScienceDirect
Deep-Sea Research II 55 (2008) 841–855
DEEP-SEA RESEARCH PART II
www.elsevier.com/locate/dsr2

^{234}Th-based export fluxes during a natural iron fertilization experiment in the Southern Ocean (KEOPS)

N. Savoye[a,*], T.W. Trull[b], S.H.M. Jacquet[a,1], J. Navez[a,c], F. Dehairs[a]

[a]Department of Analytical and Environmental Chemistry, Vrije Universiteit Brussel, Pleinlaan 2, B-1050 Brussels, Belgium
[b]CSIRO Marine and Atmospheric Research, ACE CRC and IASOS, University of Tasmania, P.O. Box 80, Hobart 7001 Australia
[c]Department of Geology, Royal Museum for Central Africa, Leuvensesteenweg 13, B-3080 Tervuren, Belgium

Accepted 8 December 2007
Available online 14 April 2008

Abstract

Five iron-fertilization experiments in the Southern Ocean have clearly demonstrated that adding iron increases primary production, but the implications for carbon export to the ocean interior have been less clear. This reflects both observational limitations of short-term experiments and their uncertain relevance to quantifying ecosystem level processes that are likely to be structured differently under conditions of punctual versus persistent stimulation. To avoid these biases, KEOPS (KErguelen Ocean and Plateau compared Study) investigated the naturally iron-fertilized Kerguelen Plateau region in the Indian Sector of the Southern Ocean that exhibits an annual phytoplankton bloom. Here, we report particulate organic carbon (POC) and nitrogen export from this system based on the ^{234}Th approach.

Results indicate that the export fluxes were variable both on and off the Kerguelen Plateau (9.0–38.4 mmol C m^{-2} d^{-1} and 1.6–4.8 mmol N m^{-2} d^{-1}) and were in the range of values reported for natural Southern Ocean ecosystems. Export fluxes were compared at two reference stations, one above and one outside the Plateau. The station above the plateau was characterized by higher iron supply and export fluxes compared to the station outside the plateau. The difference in the export flux between these two reference stations defines the export excess induced by iron fertilization. It was 10.8 ± 4.9 mmol C m^{-2} d^{-1} and 0.9 ± 0.7 mmol N m^{-2} d^{-1} at 100 m, and 14.2 ± 7.7 mmol C m^{-2} d^{-1} and 2.0 ± 1.3 mmol N m^{-2} d^{-1} at 200 m. This POC export excess was similar to those found during other studies of artificial (SOFeX) and natural (CROZEX) iron fertilization in the Southern Ocean.

The examination of the export efficiency (defined as the ratio of export to primary production) revealed significant variability over the plateau related to the temporal decoupling of production and export during the demise of the bloom. On average, the export efficiency was lower over the plateau than in surrounding waters, suggesting that increased iron supply may increase total export but lower export efficiency. Our findings are very important for evaluating present and past carbon cycling in the Southern and global oceans and for assessing predictive scenarios of carbon cycling and budget.

Keywords: Export flux; Southern Ocean; Iron-fertilization experiment; ^{234}Th

1. Introduction

The ocean buffers global warming by absorbing a significant part of the CO_2 released in the atmosphere (Battle et al., 2000) through a combination of physical and biological processes that export carbon from the surface to the deep ocean. The Southern Ocean plays a key role acting as a net sink for atmospheric CO_2: the area south of 50°S accounts for ca. 20% of the global ocean CO_2 uptake, dominantly via the biological pump (Takahashi et al., 2002). The biological pump consists of a combination of processes starting with the uptake of CO_2 by the

*Corresponding author. Present address: OASU, UMR EPOC, Université Bordeaux 1, CNRS, Station Marine d'Arcachon, 2 rue du Pr. Jolyet, F-33120 Arcachon, France. Tel.: +33 5 56 22 39 16; fax: +33 5 56 83 51 04.
E-mail addresses: n.savoye@epoc.u-bordeaux1.fr (N. Savoye), Tom.Trull@utas.edu.au (T.W. Trull), jacquet@cerege.fr (S.H.M. Jacquet), jacques.navez@africamuseum.be (J. Navez), fdehairs@vub.ac.be (F. Dehairs).
[1]Present address: CEREGE, UMR 6635, Europôle Méditerranéen de l'Arbois, Aix-en-Provence, France.

0967-0645/$ - see front matter © 2008 Elsevier Ltd. All rights reserved.
doi:10.1016/j.dsr2.2007.12.036

phytoplankton and its transformation into particulate organic carbon (POC) along with other biogenic elements like nitrogen and silicon. The particles produced in surface ocean are either remineralized in the surface layer or exported to deeper layers where again they can be remineralized or exported deeper and even to the sea floor. As a result, carbon and associated biogenic elements can be stored for days to weeks (surface mixed layer), months (winter mixed layer), decades (mesopelagic zone), centuries to millennia (deep ocean), or even millions of years (sediments), depending on the depth of export.

The Southern Ocean is the largest high-nutrients low-chlorophyll (HNLC) area. It has been proposed that primary production of HNLC areas is limited by the micro-nutrient iron and that iron supply may control primary and export production in modern and past ocean (Martin, 1990), so-called the 'iron hypothesis'. The iron-limitation of Southern Ocean primary production has now been unequivocally demonstrated by five mesoscale *in situ* experiments—SOIREE (Southern Ocean Iron Release Experiment; Boyd et al., 2000), EisenEx (Iron Experiment; Gervais et al., 2002), SOFeX-North and South (Southern Ocean Fe Experiment; Coale et al., 2004), and EIFEX (European Iron Fertilisation Experiment; Hoffmann et al, 2006)—which have shown that adding tons of iron sulfate in Southern Ocean surface waters increases primary production and phytoplankton biomass. The fate of the phytoplankton blooms also was studied during these experiments. Although the duration of SOIREE and EisenEx was too short to see any increase of the export (Charette and Buesseler, 2000; Rutgers van der Loeff and Vöge, 2001), such an increase was reported for SOFeX-South (Buesseler et al., 2004). However, the export increase due to the iron input was low ($7\,\mathrm{mmol\,C\,m^{-2}\,d^{-1}}$). Disadvantages of 'artificial' iron experiments in the context of testing the iron hypothesis include the following: (1) iron is not directly bio-available, (2) iron release is very sudden, and (3) the experiment is limited in time and space. These disadvantages lead to a loss of a large proportion of iron (Bowie et al., 2001) and may bias extrapolation of findings to natural ecosystems because of sudden iron release and snapshot view of artificial experiments. Therefore, the possibility of investigating 'natural' iron fertilization is welcome.

It is well known, especially since the advent of satellite ocean-colour measurements, that waters surrounding oceanic islands are rich in phytoplankton biomass (e.g., Feldman, 1986). In the Southern Ocean, high-chlorophyll waters are a permanent feature during the summer months over the Kerguelen Plateau and downstream of Kerguelen Island, in an area of high iron concentration (Blain et al., 2001, 2007). This makes this area an ideal natural laboratory to study the relationships between iron supply and ecosystem structure and biogeochemistry, i.e., to perform a natural iron-fertilization experiment. The KErguelen Ocean and Plateau compared Study (KEOPS) took place during austral summer 2005 and aimed at quantifying the natural iron fertilization, describing the ecosystem structure and functioning and investigating the biogeochemical impacts. In particular, the impact of iron fertilization in boosting the biological pump and the export production was investigated.

One of the best approaches to estimate the export production (i.e., the part of the primary production which leaves the surface layer) is based on the measurement of the natural radioisotope ^{234}Th. ^{234}Th is produced in ocean water from the decay of ^{238}U, which is soluble and conservatively distributed with salinity (Chen et al., 1986). Because of its short half-life (24.1 d) and its strong adsorption on particles, the deficit of ^{234}Th with respect to ^{238}U has been used as a powerful tool to study biogenic particle export from surface waters (Coale and Bruland, 1985; Waples et al., 2006). Indeed, this deficit can be converted into ^{234}Th export flux by using an appropriate model (Savoye et al., 2006), and then C and N fluxes can be estimated by multiplying the ^{234}Th flux by the C/^{234}Th and N/^{234}Th ratios of sinking particles (Buesseler et al., 1992, 2006).

The present study reports KEOPS export fluxes of POC and nitrogen (PON). We then compare HNLC and Fe-enriched waters to assess the increase in export fluxes due to natural iron fertilization during KEOPS, and contrast these results with other artificial and natural iron-fertilization results from the Southern Ocean ecosystems. In particular, we examine variations in the export efficiency—defined as the ratio of export to primary production. We conclude with discussion of the potential usefulness of the export excess and export efficiency derived from Fe-fertilization experiments to constrain models of past, modern, and future carbon cycles in the Southern and global ocean.

2. Material and methods

2.1. Study site and sampling strategy

KEOPS was carried out over Kerguelen Plateau, near Kerguelen Island, Southern Ocean (Fig. 1). It took place during the austral summer (19 January–13 February 2005) at the time of a 3-month period of high chlorophyll concentrations (Blain et al., 2007). Three transects were sampled for physics (11 stations per transect), stock parameters (six stations per transect) and flux estimations (three or less stations per transect). Two stations were visited several times and represent reference stations for Fe-supplied (A3) and HNLC (C11) waters (Fig. 1). At the time of the cruise, Fe vertical supply was an order of magnitude higher at A3 than at C11 (Blain et al., 2007). This iron supply was accompanied by inputs of major nutrients as evidenced by high diffusion coefficients (Park et al., 2008) and increasing nutrient concentration with depth (Mosseri et al., 2008). During KEOPS, dissolved iron concentration was 0.090 ± 0.034 and 0.073 ± 0.014 nM (Blain et al., 2008), chlorophyll a concentration was

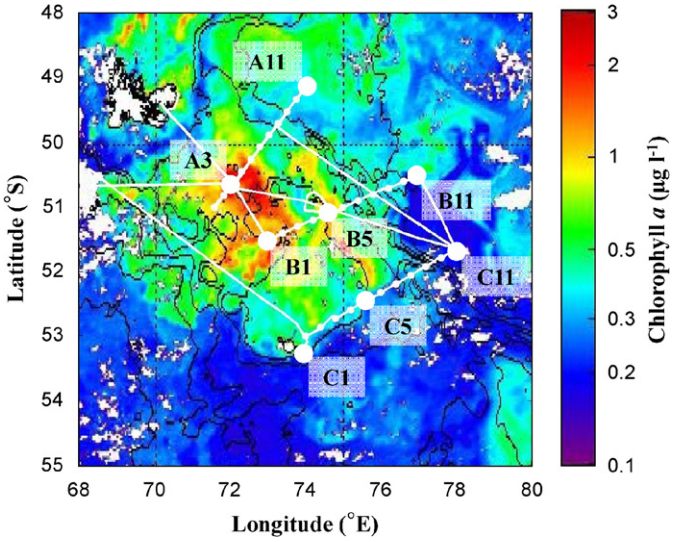

Fig. 1. Satellite image of the bloom during the KEOPS cruise. Track of the cruise (white line), position of the stations (white dots), and bathymetry (black lines).

0.35–2.8 and 0.16–0.37 µg L^{-1} (Mosseri et al., 2008; N. Garcia, personal communication) and primary production was 15–51 and 3.3–4.3 mg m^{-3} d^{-1} (Mosseri et al., 2008; N. Garcia, personal communication) in surface water of plateau stations and HNLC station C11, respectively. Phytoplankton abundance and biomass was highly dominated by diatoms at all stations; however, phytoplankton and diatom composition was station specific (Armand et al., 2008).

Within the scope of the present work, export production was studied at stations A3, A11, B1, B5, B11, C1, C5, and C11 (Fig. 1) using the ^{234}Th-deficit approach. The bloom reference station A3 was visited three times (23 January, 3 and 12 February 2005) and the HNLC reference station C11 twice (26 January and 5 February 2005). The other stations were visited once. In the following, the different visits to A3 and C11 will be differentiated as A3-3, A3-4, and A3-5, and as C11-1 and C11-2.

2.2. Total ^{234}Th activity

Four litres of seawater were sampled for total ^{234}Th using Niskin bottles at 15–16 depths between surface and 800 m for open-ocean stations (A11, B11, and C11), and at 7–14 depths between surface and 20–80 m above seafloor for plateau stations (A3, B1, B5, C1, and C5). In addition, triplicates of 2000 m water were sampled at each visit to open-ocean stations for calibration purposes.

Seawater was processed for total ^{234}Th following the double-spike method of Pike et al. (2005). Seawater was acidified to pH 2 using concentrated HNO_3 and ^{230}Th yield monitor was added to estimate ^{234}Th recovery by Mn precipitation. After 12-h equilibration period, pH was brought up to 8.5 using concentrated NH_3. $KMnO_4$ and $MnCl_2$ were added to form a precipitate and the samples were allowed to stand for 12 h before filtration on quartz-fiber filters (25-mm diameter). Filtered precipitates were dried and counted using low-level beta counters (Risø, Denmark) until counting uncertainty was below 2%. Filters were re-counted for beta background determination after a delay of six ^{234}Th half-lives. After background counting, 56% of the samples (including all 2000 m samples) were processed for ^{230}Th measurement following Pike et al. (2005) and using ^{229}Th as a tracer. ^{230}Th and ^{229}Th were measured using HR-ICP-MS (Element 2, Thermo Finnigan MAT, Germany) in low-resolution mode. Th recovery of the remaining 44% samples was estimated using the average recovery of neighboring samples. ^{234}Th overall uncertainty was 0.07 dpm L^{-1}, as determined by the median of 2000 m-triplicates standard deviations. ^{238}U activity was calculated as follows: ^{238}U (dpm L^{-1}) = 0.0686 × salinity × density (Chen et al., 1986).

2.3. ^{234}Th flux and models

C1 was a very shallow station at which the whole water column was well mixed (Fig. 2). In such an environment, ^{234}Th removal is due both to particles sinking from the surface and to particles that are resuspended from the sediment (Waples et al., 2006). As the present study is focused on export production, no export flux was calculated at C1.

At all other stations, ^{234}Th flux was calculated from ^{234}Th and ^{238}U activities using a 1D one-box model where the one-box corresponds to total ^{234}Th (Broecker et al., 1973; Buesseler et al 1992). The mass balance equation is as follows:

$$\frac{\partial^{234}\mathrm{Th}}{\partial t} = \lambda^{238}\mathrm{U} - \lambda^{234}\mathrm{Th} - P + V \quad (1)$$

where $\partial^{234}\mathrm{Th}/\partial t$ is the change of total ^{234}Th activity over time; λ is the ^{234}Th decay constant (0.02876 d^{-1}); ^{234}Th and ^{238}U are ^{234}Th and ^{238}U activities, respectively; P is the net loss of ^{234}Th on sinking particles (i.e., the export flux of ^{234}Th); and V is the ^{234}Th vertical diffusion.

Equation (1) can be solved considering either steady-state (SS) or non-steady state (NSS) conditions, i.e., considering $\partial^{234}\mathrm{Th}/\partial t$ is nil or not. SS and NSS solutions are Eq. (2) and (3), respectively,

$$P = \lambda(^{238}\mathrm{U} - {}^{234}\mathrm{Th}) + V \quad (2)$$

$$P = \lambda\left[\frac{^{238}\mathrm{U}(1-\mathrm{e}^{-\lambda\Delta t}) + {}^{234}\mathrm{Th}_1\mathrm{e}^{-\lambda\Delta t} - {}^{234}\mathrm{Th}_2}{1-\mathrm{e}^{-\lambda\Delta t}}\right] + V \quad (3)$$

where $^{234}\mathrm{Th}_1$ and $^{234}\mathrm{Th}_2$ are the ^{234}Th activity at successive visits of a single site (i.e., of a single water mass) and Δt is the time delay between the two visits.

The use of the NSS solution implies that a station has been visited at least twice. Consequently, ^{234}Th export flux was calculated using the SS solution at stations A11, B1, B5, B11, and C5 which were visited only once, and using NSS solution at stations A3 and C11, which were visited

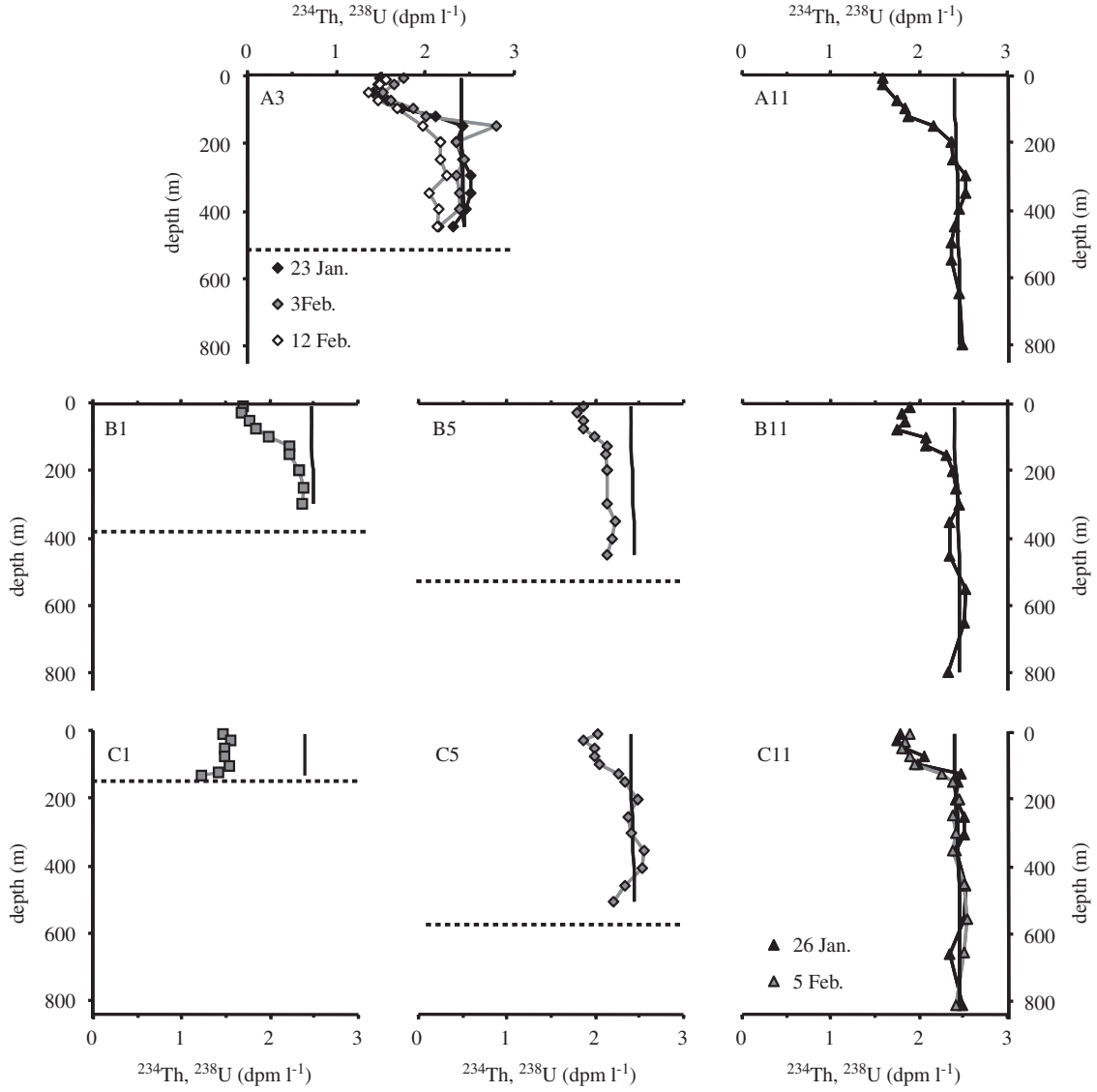

Fig. 2. Depth profiles of ^{234}Th and ^{238}U activities along transects A (upper panels), B (middle panels), and C (lower panels). Black vertical lines without symbol correspond to ^{238}U activity profiles. Dashed horizontal lines represent sea floor. Squares, diamonds, and triangles correspond to stations 1, 3 or 5, and 11, respectively. Closed black and gray symbols are stations sampled on 23 January and 3 February, respectively, $\pm$5 days. These dates correspond to the two first sampling dates of station A3. Open black symbol is the last sampling of station A3 (12 February). ^{238}U activity was calculated from salinity. Overall uncertainty of ^{234}Th activity was 0.07 dpm L^{-1}, as determined by the median of 2000 m-triplicates standard deviations. All data are reported in Supplementary Table 1.

three times and twice, respectively. Note that the time delay between consecutive visits of station A3 or C11 was 9–11 days, i.e., within the range of 1–4 weeks as recommended by Savoye et al. (2006) for the use of the NSS model.

The vertical diffusive flux (V) was estimated using the vertical gradient of total ^{234}Th activity and the K_z diffusion coefficient calculated at stations A3 and C11 from Thorpe scale measurements (Park et al., 2008). A3 and C11 K_z values were identical and were considered to apply to all stations. Using the gradient of total ^{234}Th instead of the sparser dissolved (i.e., total-particulate) ^{234}Th concentrations to correct for the diffusive supply of dissolved ^{234}Th slightly (~10% based on particulate/dissolved ^{234}Th ratios) overestimates this supply (V) and thus the export flux (P) as shown in Eqs. (2) and (3), but has the advantage of better spatial resolution. Given the other uncertainties in estimating the flux, we have made no correction for this minor bias.

2.4. Particulate ^{234}Th, POC, and PON

As explained in Section 1, ^{234}Th export flux can be converted into POC and PON export flux by multiplying the former by the POC:^{234}Th and PON:^{234}Th ratios of sinking particles. We collected particles via large-volume filtration using an *in situ* impeller pump that returns water to the deck via a hose (Trull and Armand, 2001) and via free-drifting sediment traps. Using the impeller pump,

particles were sampled from four depths (20, 60, 100, 130 m) in and just below the mixed layer at six sites (A3, A11, B5, B11, C5, and C11, plus a single 20-m sample at station C1). The pump provides ca. 50 L per minute flow through a 40-mm diameter hose to a manifold from which smaller fractions of the flow are diverted at lower pressure to the filtration system; the remainder is available for other studies (e.g., Ra isotopes, Van Beek et al., 2008) or is returned directly to the sea. The water passes through a cascade of a 47-mm diameter 1000-μm pre-screen to remove large zooplankton, followed by 142-mm diameter nylon screens (335, 210, 55, 20, and 5-μm mesh sizes) and a final 142-mm diameter QMA quartz fiber filter (1-μm nominal pore size). The flow path allows a larger flow rate through the larger meshes, so that during the ca. 1 h of filtration at each depth, 50–150 L passed through the QMA filter at ca. 1–3 L per minutes while 200–600 L passed through the 335 and 210-μm meshes. At most, a few large euphausids were obtained on the pre-screen and this material was not analyzed. The particles on the other screens were immediately resuspended and refiltered onto 25-mm diameter 1.2-μm pore size silver filters. Silver filters (size fractions larger than 5 μm) along with the QMA filters (size class 1–5 μm) were dried at 60 °C and then counted for ^{234}Th. After counting, filters were analyzed for POC and PON. The POC and PON concentrations are reported in Trull et al. (2008). Here, we report the POC:^{234}Th, PON:^{234Th}, and POC:PON ratios of particle size classes 1–5, 5–20, 20–55, 55–210, 210–335, and 335–1000 μm (Supplementary Table 2).

Particles also were sampled using sediment traps deployed at 200 m depth at stations A3 and C5. Sinking particles were collected with a cylindrical sediment trap suspended at 200 m depth beneath a free-drifting surface float equipped with an ARGOS beacon and a strobe light. This trap was successfully deployed three times (twice at A3, and once at C5), following loss of other traps during earlier deployments, and thus provides only a small set of observations. On each occasion, the trap was deployed for ca. 24 h and drifted a relatively small distance (ca. 10 km) in comparison to the dimensions of the studied features. Further details of the deployment dates and trap drifts are provided in Ebersbach and Trull (2008). The trap consists of a 2-m-long polyester-resin cylinder with a 0.125-m^2 collection area and an internal conical funnel that transfers the sinking particles to a carrousel of collection cups (PPS3/3 trap, Technicap Inc., France, www.technicap.com). Four cups (filled with trace-metal-clean brine with salinity ca. 60 prepared by freezing local sub-surface seawater but no poison because of the short deployments in cold water) were rotated beneath the funnel during each deployment for periods of a few hours. Two of these were used for trace metal studies and two were used for the nitrogen and carbon analyses reported here and the nitrogen and carbon isotopic analyses reported in Trull et al. (2008). On recovery, the cup solutions were filtered through a 350-μm nylon mesh to separate zooplankton 'swimmers'. The materials on this mesh were vigorously sprayed with a jet of seawater (pre-filtered through a 1-μm quartz filter) to disperse fecal pellets and wash them and any material clinging to the zooplankton through the mesh. Both the >350 and <350-μm size fractions were refiltered onto 25-mm 1.2-μm silver filters and dried and analyzed following the same procedures as for the suspended particles.

For ^{234}Th analyses, the 25-mm silver filters were dried and counted on board using low-level beta counters (Risø) till counting uncertainty was below 2% or during 12–30 h. The 142-mm quartz fiber filters carrying the 1–5 μm particle size fraction sampled with the impeller pump were dried, punched (25-mm diameter) and then counted for 12–30 h. All filters were re-counted for beta background determination after a delay of six ^{234}Th half-lives.

Beta counting has the advantage of being non-destructive, allowing the counted samples to be analyzed for POC and PON. The POC and PON analyses were carried out at the Central Sciences Laboratory at the University of Tasmania. Sub-samples of the 25-mm silver filters were punched and placed in silver cups, treated with 10-μl aliquots of 1 N HCl and heated at 60 °C to remove carbonates, and then with de-ionized water to remove the acid and dried a final time at 60 °C. These samples were analyzed with a Fisons combustion-gas-chromatography elemental analyser by reference to acetanilide standards. Precision of the analyses is ca. 1%, but the overall precision was limited to 5–10% by the sub-sampling of the filters.

3. Results

3.1. ^{234}Th activity profiles

^{234}Th activity was low within the upper 100 m (1.37–2.08 dpm L^{-1}), then increased with depth and reached equilibrium with ^{238}U at 125–200 m for most of the stations (all open-ocean stations, A3-3, A3-4, and C5; Fig. 2). At these stations, ^{234}Th activity was close to equilibrium until at least 800 m (open-ocean stations: A11, B11, and C11) or tens of meters above the seafloor (Plateau stations: A3-3, A4-4, and C5—one exception is the unexpected high ^{234}Th activity measured at 150 m for A3-4). Such a variation with depth—deficit in surface and equilibrium at depth—is the typical pattern encountered in open-ocean and especially in the Southern Ocean (e.g., Buesseler et al., 2001; Rutgers van der Loeff et al., 2002a). In contrast, at most of the plateau stations (A3-5, B1, B5, and C1), ^{234}Th activity never reached equilibrium at depth and remained in deficit with respect to ^{238}U. This pattern is typical of coastal and shelf waters (e.g., Charette et al., 2001; Waples et al., 2006). ^{234}Th activity also decreased with depth within the bottom layer at most of the plateau stations. Such bottom-water ^{234}Th deficit is typical for the deepest tens or even hundreds of meters and is due to ^{234}Th removal by re-suspended particles (Rutgers van der Loeff et al., 2002b; Waples et al., 2006).

Mixed-layer ^{234}Th deficit with respect to ^{238}U roughly decreased in the off-shelf direction along each transect (e.g., from B1 to B11) and from transect A to transect C (Fig. 2). C1 was the shallowest station (seafloor at 150 m depth) and was highly depleted in ^{234}Th over the whole shallow water column, similarly to what is usually observed in coastal waters (e.g., Charette et al., 2001; Waples et al., 2006).

Stations A3 and C11 were visited three and two times, respectively, and contrasted in their temporal evolution: ^{234}Th activity remained quite constant over time at C11 whereas it varied largely over depth and time at A3 (Fig. 2).

3.2. ^{234}Th fluxes

Total ^{234}Th fluxes at 100 m depth ranged from 1499 dpm m^{-2} d^{-1} at C5 to 2999 dpm m^{-2} d^{-1} at A3 (mean value), with a larger range observed at 200 m depth (1443–5217 dpm m^{-2} d^{-1} at these same sites) (Table 1; Fig. 3). These data are within the range of values reported in the literature for the Southern Ocean (Table 2). Spatial variations of fluxes are very similar to spatial variation of ^{234}Th deficit (Section 3.1), roughly decreasing from stations 1 to 11 and from transect A to C. Total ^{234}Th fluxes increased or remained rather constant with depth (taking into account associated uncertainties). Total ^{234}Th (Fig. 3) flux was mainly carried by the steady-state (SS) contribution (on average 89% of the total ^{234}Th fluxes). The contribution of vertical diffusion was low (0–11%) and fell within the uncertainty of the total ^{234}Th flux. Note that vertical diffusion of ^{234}Th decreased with depth (Fig. 3). However, NSS fluxes were only estimated at A3 and C11, the two re-visited stations. NSS contribution to total ^{234}Th flux was negligible at 100 m (C11 and mean A3 fluxes) and was ca. 30% at 200 m. However, there was a huge temporal variability of the NSS contribution at A3 since it was −1216 and 1671 dpm m^{-2} d^{-1} at 100 m, and −100 and 3825 dpm m^{-2} d^{-1} at 200 m during the study periods; thus, total ^{234}Th fluxes were 1571 and 5169 dpm m^{-2} d^{-1} at 100 m, and 2989 and 8077 dpm m^{-2} d^{-1} at 200 m during the study periods (Table 1). The maximal flux of 5169 and 8077 dpm m^{-2} d^{-1} at 100 and 200 m, respectively, are the highest ever recorded in a natural Southern Ocean ecosystem (Table 2). Note that the unusually high ^{234}Th value at A3 (A3-4, 150 m; see Section 3.1) was not used to calculate fluxes at 150 and 200 m. Indeed, including that value in the calculation results in the 200-m flux being negative between the first and the second visit, while between the second and the third visit, on the contrary, the flux would be even higher than presently calculated. However, the mean flux integrated over time would not change (Fig. 3).

3.3. C and N to ^{234}Th ratios of particles

Six size classes of particles (1–5, 5–20, 20–55, 55–210, 210–335, and 335–1000 μm) were sampled within and below the mixed layer using the hose pump. Particles were also collected at 200 m using sediment trap at stations A3 and C5. C:Th and N:Th ratios of particles were highly variable ranging from 0.2 to 1554 and from 0.02 to 257 μmol dpm^{-1}, respectively, with no overall depth or site related trend when all data are put together (Fig. 4 and Supplementary Table 2). However, C:Th and N:Th ratios roughly increased with particle size. Considering that Th adsorbs on particle surface and that POC and PON are present within the whole particle, C:Th and N:Th ratios more or less represent volume to surface area ratio, which increases with particle size (Buesseler et al., 2006).

4. Discussion

4.1. C and N to ^{234}Th ratios of sinking particles

As explained in Sections 1 and 2.4, ^{234}Th export flux can be converted into POC and PON export fluxes at a given depth horizon by multiplying the ^{234}Th flux by the C:Th and N:Th ratios of 'sinking' particle at the same depth horizon (Buesseler et al., 1992). One challenge is to catch 'sinking' particles. Among the different devices commonly used to sample particles (see Buesseler et al., 2006 and Rutgers van der Loeff et al., 2006) we used a sediment trap and a pump for large volume size fractionated filtrations.

The sediment trap was deployed twice at A3 and once at C5, at the 200 m depth horizon. Since there was no significant difference between results of both deployments at A3 (5.1 ± 1.4 and 4.3 ± 2.2 μmol dpm^{-1}, and 0.69 ± 0.20 and 0.61 ± 0.44 μmol dpm^{-1} for C:Th and N:Th, respectively; Supplementary Table 2) the average ratios were used to calculate POC and PON fluxes. At C5, C:Th and N:Th ratios were 1.6 ± 0.2 and 0.24 ± 0.04 μmol dpm^{-1}, respectively.

The hose pump was deployed between the surface and 130 m. The usual underlying assumption with size-fractionated filtration is that the larger-particle size class (e.g., >70 μm, Cochran et al., 2000; >60 μm, Coppola et al., 2005; >54 μm, Buesseler et al., 2005) represents the sinking particles. However, inspection under a stereo-microscope at 50 × revealed that the two largest size fractions (210–335 and 335–1000 μm) were largely dominated by zooplankton (Trull et al., 2008). In addition, the two largest fractions exhibited low C:N ratios (Fig. 4) and high δ^{15}N (Trull et al., 2008) at all stations, indicating the influence of heterotrophs in these size fractions—C:N ratio of zooplankton and bacteria is typically between 3 and 6 (Sterner and Elser, 2002) and δ^{15}N increases with trophic level (Owens, 1987). As zooplankton cannot be considered to represent 'sinking' particles the 210–335 and 335–1000-μm size classes were not considered for estimating C:Th, and N:Th ratios of sinking particles. Taking them into account would have biased the estimation of the ratios toward high values (Fig. 4).

During the cruise, sediment traps were also deployed with tubes containing gels in order to qualitatively analyze sinking particle composition. Results indicate that

Table 1
^{234}Th, POC, and PON export fluxes and best estimates of POC:^{234}Th (C:Th) and PON:^{234}Th (N:Th) ratios, and carbon and nitrogen export efficiency (ThE_C and ThE_N, respectively) during KEOPS

Station	Date	Depth (m)	^{234}Th flux ($dpm\,m^{-2}\,d^{-1}$)	C:Th ($\mu mol\,dpm^{-1}$)	POC flux ($mmol\,m^{-2}\,d^{-1}$)	ThE_C (%)	N:Th ($\mu mol\,dpm^{-1}$)	PON flux ($mmol\,m^{-2}\,d^{-1}$)	ThE_N (%)
A3[a]	23 January	100	3067±323						
A3[a]	23 January	150	3131±235						
A3[2]	23 January	200	3037±198						
A3[a]	3 February	100	2539±244						
A3[a]	3 February	150	3054±181						
A3[a]	3 February	200	3097±238						
A3[a]	12 February	100	3319±219						
A3[a]	12 February	150	3898±235						
A3[a]	12 February	200	4170±248						
A3[b]	23 January–3 February	100	1365±503	7.7±0.9	10.5±4.0	13	0.96±0.11	1.3±0.5	13
A3[b]	23 January–3 February	150	2917±622	5.5±0.7	16.1±4.0		0.65±0.11	1.9±0.5	
A3[b]	23 January–3 February	200	2949±772	4.7±1.6	13.9±5.9		0.65±0.28	1.9±1.0	
A3[b]	3–12 February	100	5014±590	7.7±0.9	38.4±6.3	48	0.96±0.11	4.8±0.8	55
A3[b]	3–12 February	150	6830±768	5.5±0.7	37.6±6.3		0.65±0.11	4.4±0.9	
A3[b]	3–12 February	200	8016±949	4.7±1.6	37.7±13.3		0.65±0.28	5.2±2.4	
A3[b]	**23 January–12 February**	**100**	**2999±383**	**7.7±0.9**	**23.0±3.6**	**28**	**0.96±0.11**	**2.9±0.4**	**31**
A3[b]	**23 January–12 February**	**150**	**4669±486**	**5.5±0.7**	**25.7±3.6**		**0.65±0.11**	**3.0±0.5**	
A3[b]	**23 January–12 February**	**200**	**5217±602**	**4.7±1.6**	**24.5±6.8**		**0.65±0.28**	**3.4±1.2**	
A11[a]	20 January	100	2380±164	11.0±1.2	26.3±3.3		1.67±0.18	4.0±0.5	
A11[a]	20 January	150	3096±232	6.3±0.7	19.5±2.5		0.87±0.09	2.7±0.3	
A11[a]	20 January	200	3087±233	6.3±0.7	19.4±2.5		0.87±0.09	2.7±0.3	
B1[a]	2 February	100	2322±230	6.8±0.8	15.9±2.5		1.01±0.05	2.3±0.3	
B1[a]	2 February	150	2672±168	5.1±1.0	13.5±2.7		0.69±0.13	1.8±0.4	
B1[a]	2 February	200	2829±190	4.7±1.6	13.3±4.5		0.65±0.28	1.8±0.8	
B5[a]	30 January	100	1856±211	6.8±0.8	12.7±2.1	16	1.02±0.12	1.9±0.3	21
B5[a]	30 January	150	2250±184	5.5±0.7	12.5±1.9		0.79±0.12	1.8±0.3	
B5[a]	30 January	200	2801±274	4.7±1.6	13.2±4.6		0.65±0.28	1.8±0.8	
B11[a]	28 January	100	1878±234	5.9±0.7	11.1±1.8		0.87±0.10	1.6±0.3	
B11[a]	28 January	150	2105±202	4.3±0.5	9.0±1.3		0.66±0.07	1.4±0.2	
B11[a]	28 January	200	2085±238	4.3±0.5	8.9±1.4		0.66±0.07	1.4±0.2	
C1[a]	8 February	100	–	–	–		–	–	
C5[a]	7 February	100	1499±192	6.0±0.6	9.0±1.5	21	1.05±0.11	1.6±0.3	22
C5[a]	7 February	150	1665±201	3.1±0.3	5.1±0.8		0.48±0.05	0.8±0.1	
C5[a]	7 February	200	1443±197	1.6±0.2	2.3±0.4		0.21±0.04	0.3±0.1	
C11[a]	26 January	100	1840±257						
C11[a]	26 January	150	1672±207						
C11[a]	26 January	200	1566±223						
C11[a]	5 February	100	1861±227						
C11[a]	5 February	150	1934±208						
C11[a]	5 February	200	1728±194						
C11[b]	**26 January–5 February**	**100**	**2003±503**	**6.1±0.7**	**12.2±3.3**	**58**	**0.98±0.11**	**2.0±0.5**	**37**
C11[b]	**26 January–5 February**	**150**	**2630±653**	**4.5±0.5**	**11.9±3.2**		**0.61±0.07**	**1.6±0.4**	
C11[b]	**26 January–5 February**	**200**	**2281±800**	**4.5±0.5**	**10.3±3.8**		**0.61±0.07**	**1.4±0.5**	

Bold lines correspond to NSS fluxes for the whole study period; These data were used to calculate export excess (see Section 4.2).
[a]Steady-state fluxes.
[b]Non-steady state fluxes.

zooplankton fecal pellets significantly contributed to the export flux (Ebersbach and Trull, 2008). Since no pellets were observed on the size-fraction filters, this suggests that the pumping system fragmented them into smaller particles. This made us select smaller size fractions than usually considered (>54, 60 or 70 μm) to estimate the element to ^{234}Th ratios of 'sinking' particles. However, the smallest fraction (QMA-5 μm) was not used for the estimation because (1) particles from this fraction are too small to sink, (2) QMA filters are known to adsorb dissolved ^{234}Th (Benitez-Nelson et al., 2001), and (3) this fraction represented up to 90% of total particulate ^{234}Th whereas it represented at maximum 8% and 12% of total PON and POC, respectively. These three conditions would have highly biased the ratio estimates towards low values (Fig. 4). Finally, we selected the 5–210-μm size fraction

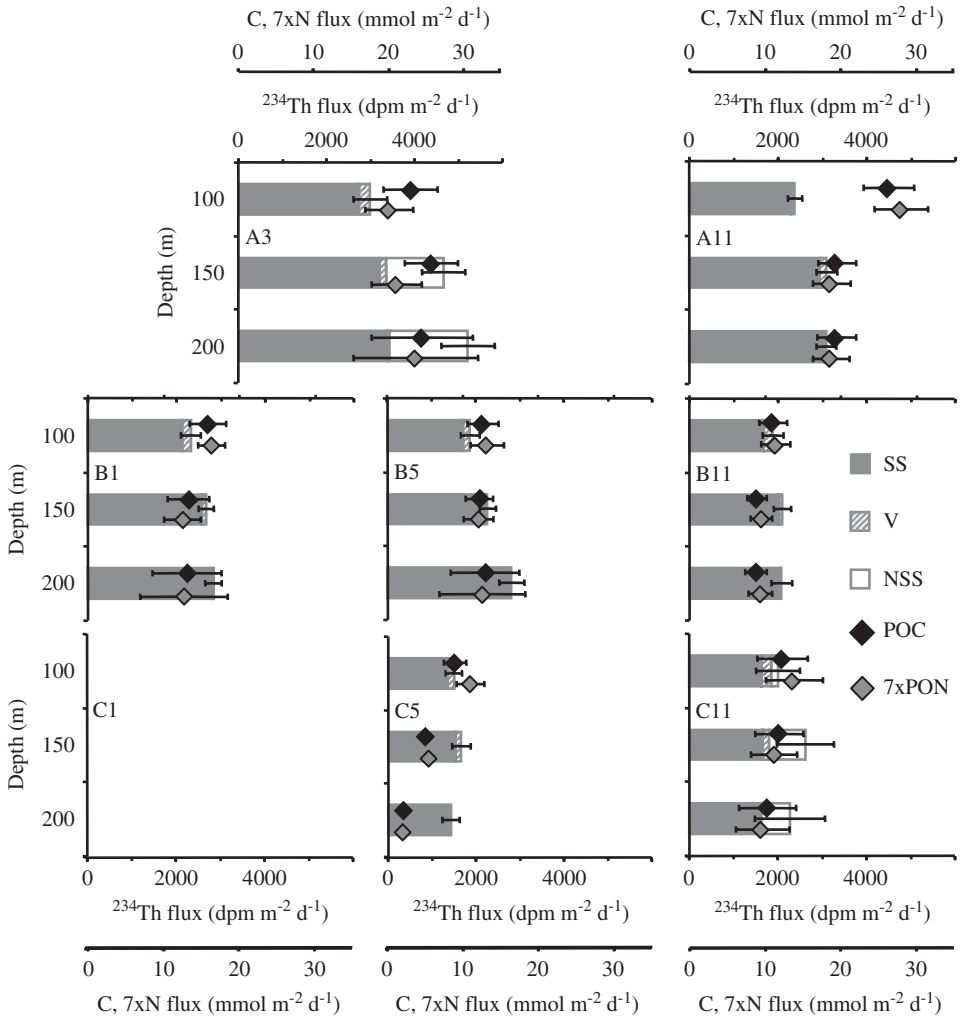

Fig. 3. ^{234}Th, POC and PON export fluxes at 100, 150 and 200 m along transects A (upper panels), B (middle panels), and C (lower panels). SS, *V*, and NSS correspond to the SS, the vertical diffusion, and the NSS contributions of the total ^{234}Th flux, respectively. SS is the first term of the right part of Eq. (2). The NSS contribution has been calculated as the difference between the fluxes calculated using Eqs. (2) and (3). At C11, SS is from the second visit and *V* is the average of both visits. At A3, SS is the mean of the second and the third visit and *V* is the average of the three visits. Note that steady-state conditions were assumed at A11, B1, B5, B11, and C5. Error bars are standard errors. Note that PON flux has been multiplied by a factor of 7 to fit the POC scale on *x*-axis. All data are reported in Table 1.

and the particles collected with the sediment trap to estimate C:Th and N:Th ratios of 'sinking' particles.

C:Th and N:Th ratios of 'sinking' particles ranged between 1.6 and 21.0 μmol dpm^{-1}, and between 0.2 and 4.0 μmol dpm^{-1}, respectively (Fig. 5). Spatial variability was high in surface waters and decreased with depth (Fig. 5). Especially, ratios at stations A11 and B5 were higher than ratios at other stations in the mixed layer but were similar to ratios at other stations at depth. All stations exhibited decreasing ratios with depth. Such a decrease in absolute value and variability of both ratios with increasing depth is a common feature in the global ocean (Buesseler et al., 2006). It is likely due to both preferential remineralization of C and N, and increase in ^{234}Th activity with depth (Rutgers van der Loeff et al., 2002a). Note that trap ratios nicely fit within the trend of decreasing ratios with depth seen in the pump samples (Fig. 5). Deep ratios (100–200 m) were very similar to literature results for the Southern Ocean (Table 1). The two latter points give confidence to our estimates of element to ^{234}Th ratios characterizing sinking particles.

Individual element to ^{234}Th ratios at 100 m were used to calculate POC and PON fluxes at 100 m for each station, with the exception of station B1, which could not be sampled for size-fractionated particles because of a hose pump deficiency. For this station, the average 100-m ratio of plateau stations was used. POC and PON fluxes of plateau stations at 150 m were calculated in a similar way, but ratio values at 150 m were obtained by linear extrapolation using the ratios at 130 and 200 m. Fluxes at 200 m were calculated at A3 and C5 using the respective trap ratio values. However, no trap was deployed at the other stations. Two-hundred-meter fluxes at other plateau stations (B1 and B5) were calculated using A3 trap ratio. The C5 trap ratio was not used for estimating B1 and B5 ratios at 200 m because this station experienced conditions

Table 2
^{234}Th, POC, and PON export fluxes, POC:^{234}Th (C:Th) and PON:^{234}Th (N:Th) ratios, and carbon and nitrogen export efficiency (ThE_C and ThE_N, respectively) from literature of the Southern Ocean at 100 m (except *: 200 m)

Zone/region	^{234}Th flux ($dpm\,m^{-2}\,d^{-1}$)	C:Th ($\mu mol\,dpm^{-1}$)	POC flux ($mmol\,m^{-2}\,d^{-1}$)	N:Th ($\mu mol\,dpm^{-1}$)	PON flux ($mmol\,m^{-2}\,d^{-1}$)	ThE_C (%)	ThE_N (%)	Reference
Bellingshausen Sea	1600	13.5	21			33		Shimmield et al. (1995)
PF to Weddell Sea	−100/1700	6/12	0/39			14/58		Rutgers van der Loeff et al. (1997)
Ross Sea	−300/2600	8/17	−2/91		−0.5/10	−6/111		Cochran et al. (2000), Vaillancourt et al. (2003)
SAZ to Ross Sea	1700/4000	3/14	5/44			16/122		Buesseler et al. (2001, 2005)
PF	865	10.2±0.8	8.8			26/62		Rutgers van der Loeff et al. (2002a)
SAZ to Weddell Gyre	−400/2600*	–	–					Usbeck et al. (2002)
SAZ to Southern	260/3000	–	–					Savoye et al. (2004)
SAZ to PFZ	100/1800	1.4	0.1/2.5			2/6		Coppola et al. (2005)
Kerguelen Region	1400/5000	5.9/11	9/38	0.9/1.7	1.3/4.8	13/58	13/55	Present study (KEOPS)
AZ-S (SOIREE)	0	–	0					Charette and Buesseler (2000)
PFZ (EisenEx)	0/1000	–	–					Rutgers van der Loeff and Vöge (2001)
AZ-S (SOFeX)								
Out	500/800	6.0±2.4	3.2/4.7	0.9	0.4/0.7	4/14		Buesseler et al. (2005)
In	350/2700	4.4±1	1.6/11.8	0.6	0.2/1.7	4/25		

Values are usually reported as min/max. PF, Polar Front; SAZ, Sub-Antarctic Zone; PFZ, Polar Front Zone; AZ-S, Antarctic Zone-South.

very close to HNLC conditions—lowest phytoplankton biomass (Armand et al., 2008), low primary production (N. Garcia, personal communication) and lowest 100 m export flux (Fig. 3, Table 1)—which are not representative of the plateau conditions. Finally, the open-ocean fluxes at 150 and 200 m were calculated using the element to ^{234}Th ratio at 130 m. This may have led to slightly overestimating the 200-m fluxes at A11, B11, and C11. However, note that 130-m ratios at these stations are not significantly different from trap ratios (Table 1; Fig. 5). Thus, the overestimation, if any, is likely negligible. All ratio values used for calculating fluxes are reported in Table 1.

4.2. POC and PON export fluxes

The 100-m export fluxes were highest at A3 ($38.4\,mmol\,C\,m^{-2}\,d^{-1}$ and $4.8\,mmol\,N\,m^{-2}\,d^{-1}$ between 3 and 12 February 2005) and A11 ($26.3\,mmol\,C\,m^{-2}\,d^{-1}$ and $4.0\,mmol\,N\,m^{-2}\,d^{-1}$). Hundred-meter export fluxes at other plateau stations ranged from $9.0\,mmol\,C\,m^{-2}\,d^{-1}$ and $1.6\,mmol\,N\,m^{-2}\,d^{-1}$ at C5 to $15.9\,mmol\,C\,m^{-2}\,d^{-1}$ and $2.3\,mmol\,N\,m^{-2}\,d^{-1}$ at B1. Hundred-meter export fluxes were 11.1 and $12.2\,mmol\,C\,m^{-2}\,d^{-1}$, and 1.6 and $2.0\,mmol\,N\,m^{-2}\,d^{-1}$ at B11 and C11, respectively. At A3, the 100-m export flux increased from 10.5 to $38.4\,mmol\,C\,m^{-2}\,d^{-1}$ and from 1.3 to $4.8\,mmol\,N\,m^{-2}\,d^{-1}$ between 23 January–3 February and 3–12 February, respectively. Hundred-meter C export fluxes are within the range of literature data for natural ecosystems (0–91 $mmol\,C\,m^{-2}\,d^{-1}$; Table 2). Export fluxes stayed constant (e.g., A3) or decreased with depth between 100 and 200 m (Fig. 3). Taking into account uncertainties, the decrease with depth is significant at A11 and C5 only.

A seasonal C budget based on DIC, POC, and DOC measurements has been performed for KEOPS and results in 100-m export flux estimates of 82 and $27\,mmol\,C\,m^{-2}\,d^{-1}$ at A3 and C11, respectively (Jouandet et al., 2008). These estimates are 3.6- and 2.2-fold higher than ^{234}Th-based estimates of POC export fluxes. Such a discrepancy between both approaches also was reported during SOFeX, with the DIC-based estimate being 1.7- or 5.1-fold higher than ^{234}Th-based estimate without or with taking patch dilution into account (Coale et al., 2004; Buesseler et al., 2005). One should keep in mind that DIC-based estimates have to be higher than or equal to ^{234}Th-based estimates; indeed, the ^{234}Th approach deals by essence only with POC export, whereas DIC approach deals with both POC and DOC exports. Furthermore, DIC estimates average the flux over the whole season (about 3 months) while ^{234}Th-based estimates average the flux over 20 (A3) or 10 (C11) days only. Thus, a direct comparison between both approaches as C export has limitation. The discrepancy between both estimates only indicates that the mean daily POC + DOC export over the season was higher than the mean daily POC export during the survey.

Interestingly, fluxes recorded in the bloom area during CROZEX—a Southern Ocean 'natural' iron-fertilization experiment carried out near Crozet Island slightly earlier in the season (November 2004–January 2005)—were very similar to KEOPS fluxes (13.0–$32.8\,mmol\,C\,m^{-2}\,d^{-1}$; Morris et al., 2007). Plateau C and N fluxes were usually higher than the in-patch fluxes recorded during SOFeX (Buesseler et al., 2005) but were lower than the maximum flux recorded in a natural ecosystem of the Southern Ocean (Ross Sea: Cochran et al., 2000; Table 2).

Nutrient (e.g., iron) availability, primary production, plankton abundance and composition, food web structure,

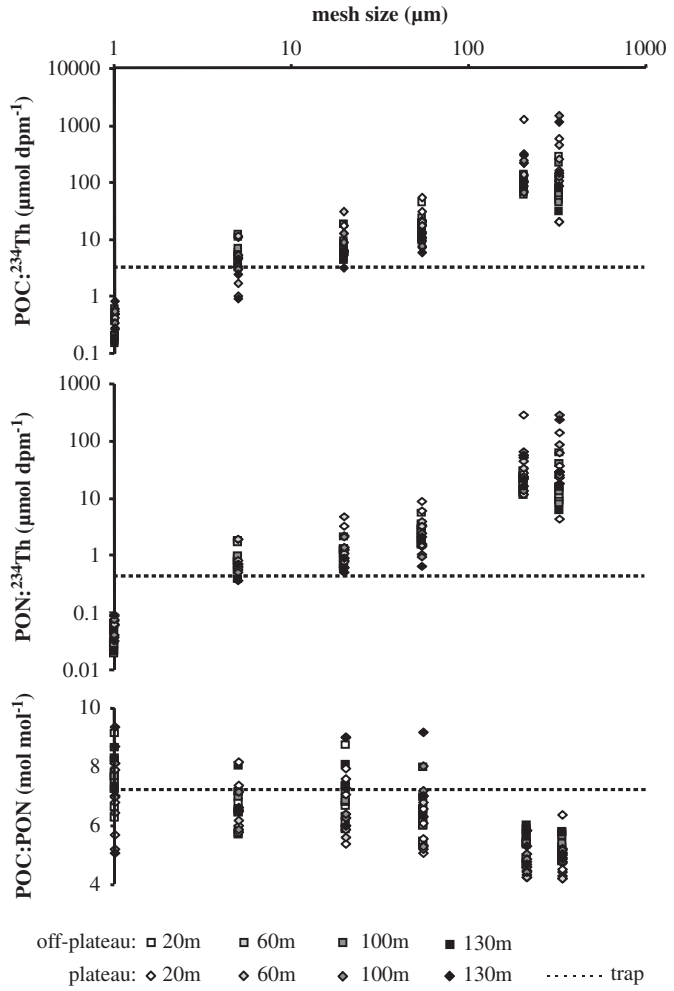

Fig. 4. Particulate organic carbon (POC) and nitrogen (PON) to ^{234}Th ratios and POC:PON ratios of particles of different size classes. The *x*-axis is mesh size of net or pore size of filter and corresponds to the following particle sizes: 1–5, 5–20, 20–55, 55–210, 210–335, and 335–1000 µm. Particles were sampled at 20, 60, 100, and 130 m depth using a large-volume filtration system (symbols) and at 200 m using sediment trap (dotted line) (see Section 2.4 for details).

etc., are parameters which are supposed to be more or less directly responsible for the magnitude of export production (Wassmann, 1998). These parameters in addition to initial conditions were different between the four experiments cited above and should explain the difference in export intensities between 'natural' and artificial iron-fertilization experiments. Furthermore, the end of the iron-induced bloom and of the export period was not witnessed during the time span of SOFeX (Coale et al., 2004; Buesseler et al., 2004)—a survey of 23 days after enrichment. Thus, the highest export flux reported during SOFeX is likely not a final maximum since the true maximal export flux may have taken place after the end of the survey period. This is corroborated by EIFEX results: the maximum of chlorophyll a concentration was recorded 26 days after the first iron infusion; chlorophyll a abruptly decreased afterward (Hoffmann et al., 2006).

The difference between the export fluxes of Fe-supplied and HNLC reference stations (A3 and C11, respectively; Blain et al., 2007) reflects the export excess induced by iron fertilization. This excess reached 10.8 ± 4.9 mmol C m^{-2} d^{-1} and 0.9 ± 0.7 mmol N m^{-2} d^{-1} at 100 m and 14.2 ± 7.7 mmol C m^{-2} d^{-1} and 2.0 ± 1.3 mmol N m^{-2} d^{-1} at 200 m. KEOPS POC export excess is similar to what was observed during SOFeX (7.1 ± 3.9 mmol C m^{-2} d^{-1} at 100 m; Buesseler et al., 2005) and the first leg of CROZEX (9.4 ± 1.5 mmol C m^{-2} d^{-1} at 100–200 m; November 11–December 3, 2004; Morris et al., 2007). However, there was no POC export excess between the 'bloom area' and 'non-bloom area' during the second leg of CROZEX (December 19, 2004–January 12, 2005).

4.3. Linking export to primary production

Linking export production to primary production represents a challenge since export production depends not only on the magnitude of primary production, but also on the type of particles, phytoplankton composition, food web structure, etc. (Wassmann, 1998; Buesseler et al., 2006). Understanding of the relationship between primary and export production is highly important for proper assessment and modeling of the global carbon cycle. Since primary production can be estimated via remote sensing, a transfer function between export and primary production would be very useful. By defining the export efficiency as the ThE ratio—the ratio of ^{234}Th-based export production to primary production—Buesseler (1998) examined this relationship. The author reported ThE ratios varying between almost zero and more than 50%. Most of the ThE values fall between 2% and 10%; the highest values (>10%) were mainly associated with high-latitude blooms and occasionally also mid-latitude spring blooms, and were attributed to the sinking of large phytoplankton cells such as diatoms. Since that study, ThE ratios exceeding 100% (i.e., export production > primary production) have been reported for the Southern Ocean (Buesseler et al., 2003; Savoye, Trull and Buesseler, unpublished data), indicating a decoupling between both processes.

Decoupling between primary production (PP) and export production (EP) not only appears at the spatial scale but also at the seasonal scale. Indeed, one can summarize a bloom cycle as consisting of the following four stages—(0) bloom limited conditions (e.g., during winter): low PP, low/no EP; (1) start of the bloom: high PP, low/no EP (low ThE); (2) maximum of the bloom: high PP, high EP; (3) demise of the bloom: low PP, high EP (ThE > 1). This pattern is in fact a simplistic view of complex interactions between EP and PP (Wassmann, 1998 and references therein).

Furthermore, iron availability to phytoplankton may partly control export efficiency. For instance, Southern Ocean AESOPS results indicate that ThE was highest (>50%) at the southernmost stations where iron stress was presumably highest (Buesseler et al., 2003); during

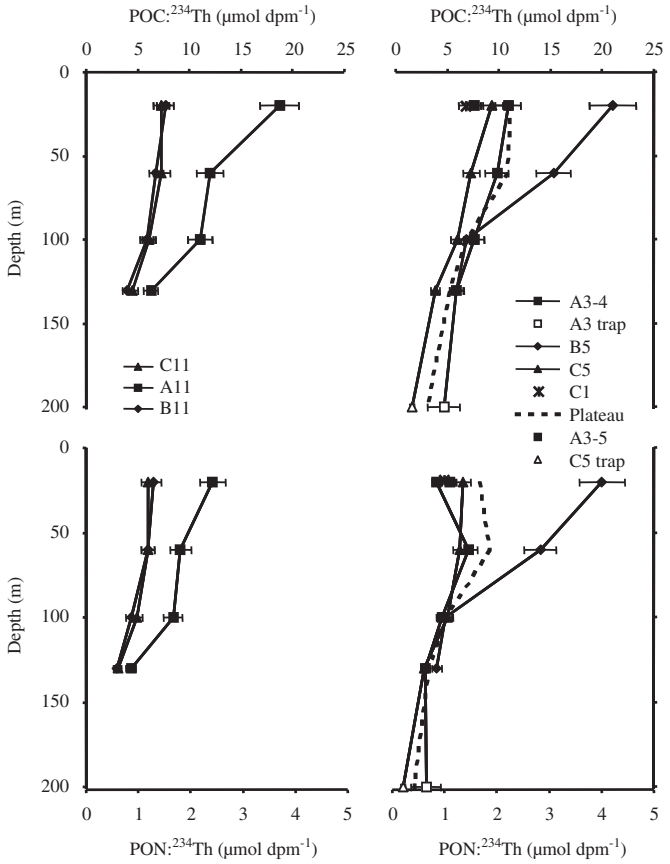

Fig. 5. Estimates of particulate organic carbon (POC; upper panels) and nitrogen (PON; lower panels) to ^{234}Th ratios of 'sinking' particles over depth. Left panels: off-plateau stations; Right panels: plateau stations. Particles were collected using a large-volume pumping system (size fraction: 5–210 μm; depths: 20, 60, 100, and 130 m; closed symbols) and sediment trap (200 m; open square and triangle). Also indicated are plateau average values (dashed line). Error bars are propagated uncertainty (pump data) or standard deviation of replicates (trap; two trap deployments at A3 and one trap deployment at C5; two tubes per deployment).

SOFeX, the export efficiency increased from 4% before iron release to 14% and 25% at the end of the experiment in- and out-patch, respectively. Here, we investigate export efficiency at stations A3 (Fe-supplied reference station), C11 (HNLC reference station), B5, and C5, where primary production and N-uptake rate were measured during KEOPS (Mosseri et al., 2008; N. Garcia, personal communication). We distinguish the POC export efficiency (ThE_C, defined as above) and the PON export efficiency (ThE_N, the ratio of PON export to N-uptake). Data are reported in Table 1. Note that we only discuss 100 m export efficiency.

POC export efficiency varied from 13% (A3; 22 January–3 February) to 58% (C11) whereas PON export efficiency varied from 13% (A3; 22 January–3 February) to 55% (A3; 3–12 February). ThE_C values are high (>10%) and in agreement with literature data for the Southern Ocean (Buesseler, 1998; Table 2). At A3, export efficiency strongly increased over time (ThE_C from 13% to 48%; ThE_N from 13% to 55%). This increase is mainly due to the increase of POC and PON export (Table 1) since C- and N-uptake were very constant over time (Mosseri et al., 2008). These very high values (ca. 50%) are in close agreement with the fact that the last visit of A3 occurred at the time of the demise of a bloom (Blain et al., 2007; Armand et al., 2008). On the contrary, B5, which exhibited the lowest POC and PON export efficiencies of 16% and 21%, respectively, was sampled during the growing period of the bloom in this region (between stages 1 and 2; Mongin et al., 2008). When averaging over the survey period, A3 POC and PON export efficiencies were 28% and 31%, respectively. Thus, at the time scale of the survey, plateau stations—where conditions are supposed to be Fe-supplied—exhibited lower export efficiency than the HNLC station (58%). So, it looks like iron fertilization increases both primary (Mosseri et al., 2008) and export production but decreases the export efficiency (i.e., the percentage of primary production that is exported). Higher export efficiency in HNLC conditions compared to Fe-supplied conditions was also found during AESOPS and SOFeX (Buesseler et al., 2003, 2005).

As stated above, many factors may influence the link between primary and export production. Here, we investigate the possible role of the food web structure and functioning on the export efficiency in relation to iron conditions during KEOPS. At both A3 and C11 stations, <10 μm-phytoplankton, >10 μm-phytoplankton, and mesozooplanton biomasses were dominated by nanoplankton, diatoms, and large copepods, respectively; however, diatom biomass was dominated by larger species at A3 than at C11 (Christaki et al., 2008; Armand et al., 2008; Carlotti et al., 2008; Sarthou et al., 2008). Interestingly, at A3, large cells (>10 μm) accounted for 79% of the primary production whereas at C11 small cells (<10 μm) accounted for 72% of the primary production (Christaki et al., 2008). The main difference between the food web structures was dominance of the microbial heterotrophic community by bacteria at A3, but heterotrophic nanoplankton at C11. In addition, tintinnids—which are bacterivorous—were almost absent from the ciliate pool at C11 (Christaki et al., 2008).

In terms of food web functioning, it appeared at both sites that direct mesozooplankton grazing on plankton played a minor role in the control of the primary production (Carlotti et al., 2008); copepods were likely omnivorous grazing on ciliates and aggregates (Carlotti et al., 2008; Sarthou et al., 2008). Especially, prey–predator experiments carried out at A3 revealed low utilization of phytoplankton stock by copepods, which exhibited low daily rations (Sarthou et al., 2008). Bacteria were very active and bacterial carbon demand accounted for 45% and 124% of the gross community production at A3 and C11, respectively (Obernosterer et al., 2008; Lefèvre et al., 2008). At A3, ca. 80% of the bacterial production was rapidly respired (Obernosterer et al., 2008).

One of the main differences between A3 and C11 in terms of food web functioning was the microbial food web:

the abundance of heterotrophic nanoflagellates—which are bacterial predators—showed a significant coupling with bacterial production in the HNLC area only: heterotrophic nanoflagellates consumed 80–95% of bacterial production at C11, whereas they consumed only ca. 35% of the latter at A3 where bacterial production was likely controlled by viral lysis (Christaki et al., 2008). This implies that bacterial C transfer to higher levels was much more efficient at C11. Thus, a possible explanation for the export efficiency is that at the Fe-supplied site, little bacterial carbon reached the higher trophic levels (low consumption of bacterial production by heterotrophic nanoflagellates; viral lysis of bacteria) while at the HNLC site, primary production was efficiently transferred to higher trophic levels through the microbial food web (bacteria + heterotrophic nanoflagellates) and was thus available for export through mesozooplankton fecal pellets. This greater transfer of the primary production to higher trophic levels in the HNLC area and thus its greater availability for export through fecal pellets may explain the higher export efficiency for the KEOPS HNLC area (58%) compared to the plateau Fe-supplied area (28%) where the primary production returns mainly to the dissolved pool through bacterial respiration (DIC) and viral lysis of bacteria (DOC).

Another factor that may influence the link between primary and export production is the ballast effect—i.e., particles containing mineral phases are denser and tend to sink more rapidly (e.g., Klaas and Archer, 2002). HNLC diatoms are usually heavily silicified (Smetacek et al., 2004); during KEOPS, diatoms sampled at C11 exhibited a stronger degree of silicification than diatoms sampled at A3, although they were also smaller (Mosseri et al., 2008; Armand et al., 2008). Thus, greater silicification may have been a factor influencing the higher export efficiency at the HNLC station compared to the iron-supplied station, but given that sediment trap observations emphasize the importance of fecal pellets in the flux (Ebersbach and Trull, 2008), the efficiency of carbon transfer through the trophic web is likely to have been more important.

It should be noted that the above discussion focused on export efficiency (i.e., export relative to primary production), but that absolute export, as well as primary production, was higher at the Fe-supplied site than at the HNLC site.

Although for POC export this difference in export efficiency was large between plateau and HNLC stations ($16\% \leqslant$ plateau $ThE_C \leqslant 28\%$; HNLC $ThE_C = 58\%$), it was only small for PON export ($21\% \leqslant$ plateau $ThE_N \leqslant 31\%$; HNLC $ThE_N = 37\%$). This lower ThE_N than ThE_C at C11 indicates a higher remineralization of N relative to C at this station as compared to the other stations. It is in agreement with the fact that C11 exhibited the lowest *f*-ratio during the KEOPS cruise (Mosseri et al., 2008; Trull et al., 2008).

5. Summary and conclusions

The KEOPS cruise provided a great opportunity for studying the impact of natural iron fertilization on the biological pump. In comparison to artificial experiments, such an approach has the advantage of studying natural ecosystem functioning with established plankton and microbial communities and food webs. In this scope, the export production was investigated. Though the stations located on the Kerguelen Plateau exhibited variable export production, the plateau reference station for iron-supplied conditions exhibited higher export fluxes than the reference station for HNLC conditions. Excess POC export flux was similar to what was reported for the artificial fertilization experiment SOFeX and for the other natural fertilization experiment CROZEX. No export excess was found during earlier experiments presumably due to the short duration of the survey. However, export fluxes recorded on the Kerguelen Plateau were within the range of literature data for natural ecosystems of the Southern Ocean. The mean POC export excess of ca. $9\,mmol\,C\,m^{-2}\,d^{-1}$ recorded at 100 m and of ca. $12\,mmol\,C\,m^{-2}\,d^{-1}$ recorded at 200 m during SOFeX, KEOPS, and/or CROZEX should be very useful to better constrain models dealing with paleo-productivity and paleo-climate in the scope of the iron hypothesis and with predictive scenarios.

The examination of the export efficiency—defined as the ratio of export to primary production—revealed that it was lower in iron-supplied than iron-depleted conditions during KEOPS. A similar pattern was seen during SOFeX. This illustrates again the non-linear response of export production variation to primary production variation. This was likely due to the difference in the microbial food web functioning between both areas: while mesozooplankton grazing was low and bacterial carbon demand high relative to primary production in both areas, above the plateau most of bacterial production was respired, whereas most of it was consumed by heterotrophic nanoflagellates in the HNLC area. The latter leads to the indirect transfer of autotrophic C to higher trophic levels making it available for the export through mesozooplankton fecal pellets. Such a non-linear response of export production increase to primary production induced by iron fertilization has to be taken into account when modeling iron impact on C sequestration, both for past and predictive scenarios.

Finally, the absolute and relative increase in export production above the plateau, as compared to the off-shelf situation, is larger at 200 m than at 100 m, indicating that iron fertilization induces a deeper export. Such a conclusion is confirmed by the study of biogenic particulate barium—a proxy of carbon remineralization—in the mesopelagic layer; relative to the export production, the mesopelagic remineralization was larger at HNLC than at Fe-supply reference stations (Jacquet et al., 2008). Thus, the vertical transport efficiency is higher in iron-supplied conditions; in other words, iron reduces the export efficiency, but the flux that is exported is likely to be transported deeper in the water column under Fe-supplied conditions compared to HNLC conditions. This means that under Fe-supplied conditions, exported carbon would be sequestered for a longer time compared to HNLC

conditions. Again, future models of C sequestration should consider the impact of Fe-fertilization to transport efficiency, in addition to export efficiency, for assessing past and predictive scenarios.

Acknowledgments

Authors thank the crew of the R/V *Marion-Dufresne* for assistance on board, and Stéphane Blain and Bernard Quéguiner as chief scientists of the KEOPS program and cruise, respectively. We thank Nicole Garcia and Valérie Sandroni for making available C- and N-uptake data, Y.-H. Park and I. Durand for K_z results, making available CTD data and discussion about the physics of the plateau; and Ingrid Obernosterer, Urania Christaki, Dorothée Vincent, Géraldine Sarthou, Stéphane Blain, and Dominique Lefèvre for fruitful discussions. Steve Bray and Lisette Robertson (ACE) prepared the pump and filtration equipment. Steve Bray (ACE), Danny Mclaughlin (CMAR), Jim Valdes, and John Andrews (WHOI), and Nathalie Leblond (INSU) prepared the surface-tethered trap equipment. Friederike Ebersbach (ACE) assisted with onboard filtering. Graham Rowbottom did the POC and PON analyses in the University of Tasmania Central Sciences Laboratory. Finally, we thank Michiel Rutgers van der Loeff and Laurent Coppola whose comments and suggestions helped to improve the quality of the present manuscript.

This research was supported by the Federal Belgian Science Policy Office under SPSD Programs on Global Change, Ecosystems and Biodiversity, Brussels, Belgium (BELCANTO network contracts EV/37/7C, EV/03/7A, SD/CA/03A), the Vrije Universiteit Brussel under grant GOA22, and the Research Foundation Flanders via contract G. 0021.04, by the Australian Commonwealth Cooperative Research Centre Program, the CSIRO Marine and Atmospheric Research, and the Australian Antarctic Science Program (T. Trull et al. AAS#1156), by the French–Australian Science and Technology Cooperation (T. Trull et al. Award #FR040170), and by the French Research program of INSU-CNRS PROOF (PROcessus biogéochimiques dans l'Océan et Flux) and the French Polar Institute IPEV. Sediment trap equipment was loaned from the US NSF VERTIGO project (K. Buesseler, T. Trull et al. Award #0301139).

Appendix A. Supplementary data

Supplementary data associated with this article can be found, in the online version, at doi:10.1016/j.dsr2.2007.12.036.

References

Armand, L., Cornet-Barthau, V., Mosseri, J., Quéguiner, B., 2008. Late summer diatom biomass and community structure on and around the naturally iron-fertilized Kerguelen plateau in the Southern Ocean. Deep-Sea Research II, this issue [doi:10.1016/j.dsr2.2007.12.032].

Battle, M., Bender, M.L., Tans, P.P., White, J.W.C., Ellis, J.T., Conway, T., Francey, R.J., 2000. Global carbon sinks and their variability inferred from atmospheric O_2 and $\delta^{13}C$. Science 287, 2467–2470.

Benitez-Nelson, C., Buesseler, K.O., Rutgers van der Loeff, M., Andrews, J., Ball, L., Crossin, G., Charette, M.A., 2001. Testing a new small-volume technique for determining thorium-234 in seawater. Journal of Radioanalytical and Nuclear Chemistry 248, 795–799.

Blain, S., Tréguer, P., Belviso, S., Bucciarelli, E., Denis, M., Desabre, S., Fiala, M., Martin-Jézéquel, V., Le Fèvre, J., Mayzaud, P., Marty, J.-C., Razouls, S., 2001. A biogeochemical study of the island mass effect in the context of the iron hypothesis: Kerguelen Islands, Southern Ocean. Deep-Sea Research I 48, 163–187.

Blain, S., Quéguiner, B., Armand, L., Belviso, S., Bombled, B., Bopp, L., Bowie, A., Brunet, C., Brussaard, C., Carlotti, F., Christaki, U., Corbière, A., Durand, I., Ebersbach, F., Fuda, J.-L., Garcia, N., Jeandel, C., Gerringa, L., Griffiths, B., Guigue, C., Guillerm, C., Jacquet, S., Laan, P., Lefèvre, D., Lomonaco, C., Malits, A., Mosseri, J., Obernosterer, I., Park, Y.-Y., Picheral, M., Pondaven, P., Remenyi, T., Sandroni, V., Sarthou, G., Savoye, N., Scouarnec, L., Souhaut, M., Thuiller, D., Timmermans, K., Trull, T., Uitz, J., van Beek, P., Veldhuis, M., Vincent, D., Viollier, E., Vong, L., Wagener, T., 2007. Impacts of natural iron fertilisation on carbon sequestration in the Southern Ocean. Nature 446, 1070–1074.

Blain, S., Sarthou, G., Laan, P., 2008. Distribution of dissolved iron during the natural iron fertilisation experiment KEOPS (Kerguelen Plateau, Southern Ocean). Deep-Sea Research II, this issue [doi:10.1016/j.dsr2.2007.12.028].

Bowie, A.R., Maldonado, M.T., Frew, R.D., Croot, P.L., Achterberg, E.P., Mantoura, R.F.C., Worsfold, P.J., Law, C.S., Boyd, P.W., 2001. The fate of added iron during a mesoscale fertilisation experiment in the Southern Ocean. Deep-Sea Research II 48, 2703–2743.

Boyd, P.W., Watson, A.J., Law, C.S., Abraham, E.R., Trull, T., Murdoch, R., Bakker, D.C.E., Bowie, A.R., Buesseler, K.O., Chang, H., Charette, M., Croot, P., Downing, K., Frew, R., Gall, M., Hadfield, M., Hall, J., Harvey, M., Jameson, G., LaRoche, J., Liddicoat, M., Ling, R., Maldonado, M.T., McKay, R.M., Nodder, S., Pickmere, S., Pridmore, R., Rintoul, S., Safi, K., Sutton, P., Strzepek, R., Tanneberger, K., Turner, S., Waite, A., Zeldis, J., 2000. Phytoplankton bloom upon mesoscale iron fertilisation of polar Southern Ocean waters. Nature 407, 695–702.

Broecker, W.S., Kaufman, A., Trier, R.M., 1973. The residence time of thorium in surface sea water and its implication regarding the rate of reactive pollutants. Earth and Planetary Science Letters 20, 35–44.

Buesseler, K.O., 1998. The decoupling of production and particulate export in the surface ocean. Global Biogeochemical Cycles 12 (2), 297–310.

Buesseler, K.O., Bacon, M.P., Cochran, J.K., Livingstone, H.D., 1992. Carbon and nitrogen export during the JGOFS North Atlantic Bloom Experiment estimated from ^{234}Th:^{238}U disequilibria. Deep-Sea Research 39 (7/8), 1115–1137.

Buesseler, K.O., Ball, L., Andrews, J., Cochran, J.K., Hirschberg, D.J., Bacon, M.P., Fleer, A., Brzezinski, M., 2001. Upper ocean export of particulate organic carbon and biogenic silica in the Southern Ocean along 170°W. Deep-Sea Research II 48 (19/20), 4275–4297.

Buesseler, K.O., Barber, R.T., Dickson, M.-L., Hiscock, M.R., Moore, J.K., Sambrotto, R., 2003. The effect of marginal ice-edge dynamics on production and export in the Southern Ocean along 170°W. Deep-Sea Research II 50, 579–603.

Buesseler, K.O., Andrews, J.E., Pike, S.M., Charette, M.A., 2004. The effect of iron fertilization on carbon sequestration in the Southern Ocean. Science 304, 414–417.

Buesseler, K.O., Andrews, J.E., Pike, S.M., Charette, M.A., Goldson, L.E., Brzezinski, M.A., Lance, V.P., 2005. Particle export during the Southern Ocean Iron Experiment (SOFeX). Limnology and Oceanography 50 (1), 311–327.

Buesseler, K.O., Benitez-Nelson, C.R., Moran, S.B., Burd, A., Charette, M., Cochran, J.K., Coppola, L., Fisher, N.S., Fowler, S.W., Gardner, W.D., Guo, L.D., Gustafsson, ø., Lamborg, C.,

Masque, P., Miquel, J.C., Passow, U., Santschi, P.H., Savoye, N., Stewart, G., Trull, T., 2006. An assessment of particulate organic carbon to thorium-234 ratios in the ocean and their impact on the application of ^{234}Th as a POC flux proxy. Marine Chemistry 100, 213–233.

Carlotti, F., Thibault-Botha, D., Nowaczyk, A., Lefèvre, D., 2008. Zooplankton community structure, biomass and role in carbon fluxes during the second half of a phytoplankton bloom in the eastern sector of the Kerguelen Shelf (January–February 2005). Deep-Sea Research II, this issue [doi:10.1016/j.dsr2.2007.12.010].

Charette, M.A., Buesseler, K.O., 2000. Does iron fertilization lead to rapid carbon export in the Southern Ocean? Geochemistry, Geophysics, Geosystems, 1, 2000GC000069.

Charette, M.A., Moran, S.B., Pike, S.M., Smith, J.N., 2001. Investigating the carbon cycle in the Gulf of Maine using the natural tracer thorium 234. Journal of Geophysical Research [Oceans] 106 (C6), 11553–11579.

Chen, J.H., Edwards, R.L., Wasserburg, G.J., 1986. ^{238}U, ^{234}U and ^{232}Th in seawater. Earth and Planetary Science Letters 80, 241–251.

Christaki, U., Obernosterer, I., Van Wambeke, F., Veldhuis, M., Garcia, N., Catala, P., 2008. Microbial food web structure in a naturally iron fertilized area in the Southern Ocean (Kerguelen Plateau). Deep-Sea Research II, this issue [doi:10.1016/j.dsr2.2007.12.009].

Coale, K.H., Bruland, K.W., 1985. ^{234}Th:^{238}U disequilibria within the California current. Limnology and Oceanography 30, 22–33.

Coale, K.H., Johnson, K.S., Chavez, F.P., Buesseler, K.O., Barber, R.T., Brzezinski, M.A., Cochlan, W.P., Millero, F.J., Falkowski, P.G., Bauer, J.E., Wanninkhof, R.H., Kudela, R.M., Altabet, M.A., Hales, B.E., Takahashi, T., Landry, M.R., Bidigare, R.R., Wang, X., Chase, Z., Strutton, P.G., Friederich, G.E., Gorbunov, M.Y., Lance, V.P., Hilting, A.K., Hiscock, M.R., Demarest, M., Hiscock, W.T., Sullivan, K.F., Tanner, S.J., Gordon, R.M., Hunter, C.N., Elrod, V.A., Fitzwater, S.E., Jones, J.L., Tozzi, S., Koblizek, M., Roberts, A.E., Herndon, J., Brewster, J., Ladizinsky, N., Smith, G., Cooper, D., Timothy, D., Brown, S.L., Selph, K.E., Sheridan, C.C., Twining, B.S., Johnson, Z.I., 2004. Southern Ocean iron enrichment experiment: carbon cycling in high- and low-Si waters. Science 304, 408–414.

Cochran, J.K., Buesseler, K.O., Bacon, M.P., Wang, H.W., Hirschberg, D.J., Ball, L., Andrews, J., Crossin, G., Fleer, A., 2000. Short-lived thorium isotopes (^{234}Th, ^{228}Th) as indicators of POC export and particle cycling in the Ross Sea, Southern Ocean. Deep-Sea Research II 47 (15/16), 3451–3490.

Coppola, L., Roy-Barman, M., Muslow, S., Povinec, P., Jeandel, C., 2005. Low particulate organic carbon export in the frontal zone of the Southern Ocean (Indian Sector) revealed by ^{234}Th. Deep-Sea Research I 52, 51–68.

Ebersbach, F., Trull, T.W., 2008. Sinking particle properties from polyacrylamide gels during the KErguelen Ocean and Plateau compared Study (KEOPS): zooplankton control of carbon export in an area of persistent natural iron inputs in the Southern Ocean. Limnology and Oceanography 53 (1), 212–224.

Feldman, G.C., 1986. Patterns of phytoplankton production around the Galapagos Islands. In: Bowman, M.J., et al. (Eds.), Tidal Mixing and Plankton Dynamics, Lecture Notes Coastal Estuarine Studies. Springer, Berlin, pp. 77–106.

Gervais, F., Riebesell, U., Gorbunov, M.Y., 2002. Changes in primary productivity and chlorophyll a in response to iron fertilization in the southern Polar Frontal Zone. Limnology and Oceanography 47, 1324–1335.

Hoffmann, L.J., Peeken, I., Lochte, K., Assmy, P., Veldhuis, M., 2006. Different reactions of Southern Ocean phytoplankton size classes to iron fertilization. Limnology and Oceanography 51 (3), 1217–1229.

Jacquet, S.H.M., Dehairs, F., Savoye, N., Obernosterer, I., Christaki, U., Monnin, C., Cardinal, D., 2008. Mesopelagic organic carbon remineralization in the Kerguelen Plateau region tracked by biogenic particulate Ba. Deep-Sea Research II, this issue [doi:10.1016/j.dsr2.2007.12.038].

Jouandet, M.P., Blain, S., Metzl, N., Brunet, C., Trull, T., Obernosterer, I., 2008. A seasonal carbon budget for a naturally iron-fertilized bloom over the Kerguelen plateau in the Southern Ocean. Deep-Sea Research II, this issue [doi:10.1016/j.dsr2.2007.12.037].

Klaas, C., Archer, D.E., 2002. Association of sinking organic matter with various types of mineral ballast in the deep sea: implications for the rain ratio. Global Biogeochemical Cycles 16 (4).

Lefèvre, D., Guigue, C., Obernoster, I., 2008. The metabolic balance at two contrasting sites in the Southern Ocean: The iron-fertilized Kerguelen area and HNLC waters. Deep-Sea Research II, this issue [doi:10.1016/j.dsr2.2007.12.006].

Martin, J.H., 1990. Glacial-interglacial CO_2 change: the iron hypothesis. Paleoceanography 5, 1–13.

Mongin, M., Molina, E., Trull, T.W., 2008. Seasonality and scale of the Kerguelen plateau phytoplankton bloom: a remote sensing and modeling analysis if the influence of natural iron fertilization in the Southern Ocean. Deep-Sea Research II, this issue [doi:10.1016/j.dsr2.2007.12.039].

Morris, P.J., Sanders, R., Turnewitsch, R., Thomalla, S., 2007. ^{34}Th-derived particulate organic carbon export from an island-induced phytoplankton bloom in the Southern Ocean. Deep-Sea Research II 54 (18–20), 2208–2232.

Mosseri, J., Quéguiner, B., Armand, L., Cornet-Barthaux, V., 2008. Impact of iron on silicon utilization by diatoms in the Southern Ocean: a case study of the Si/N cycle decoupling in a naturally iron-enriched area. Deep-Sea Research II, this issue [doi:10.1016/j.dsr2.2007.12.003].

Obernosterer, I., Christaki, U., Lefèvre, D., Catala, P., Van Wambeke, F., Lebaron, P., 2008. Rapid bacterial mineralization of organic carbon produced during a phytoplankton bloom induced by natural iron fertilization in the Southern Ocean. Deep-Sea Research II, this issue [doi:10.1016/j.dsr2.2007.12.005].

Owens, N.J.P., 1987. Natural variations in ^{15}N in the marine environment. In: Blaxter, J.H.S., Southward, A.J. (Eds.), Advances in Marine biology, vol. 24. Academic Press, London, pp. 389–451.

Park, Y.-H., Fuda, J.-L., Durand, I., Naveira Garabato, A.C., 2008. Internal tides and vertical mixing over the Kerguelen Plateau. Deep-Sea Research II, this issue [doi:10.1016/j.dsr2.2007.12.027].

Pike, S.M., Buesseler, K.O., Andrews, J., Savoye, N., 2005. Quantification of Th-234 recovery in small volume seawater samples by inductively coupled plasma-mass spectrometry. Journal of Radioanalytical and Nuclear Chemistry 263 (2), 355–360.

Rutgers van der Loeff, M., Vöge, I., 2001. Does Fe fertilisation enhance the export production as measured through the ^{234}Th/^{238}U disequilibrium in surface water? In: Smetacek, V., Bathmann, U., El Naggar, S. (Eds.), The Expeditions ANTARKTIS XVIII/1-2 of the Research Vessel Polarstern in 2000. Berichte zur Polar- und Meeresforschnung, vol. 400. AWI, Bremerhaven, Germany, pp. 222–225.

Rutgers van der Loeff, M., Friedrich, J., Bathmann, U.V., 1997. Carbon export during the spring bloom at the Antarctic Polar Front, determined with the natural tracer ^{234}Th. Deep-Sea Research II 44, 457–478.

Rutgers van der Loeff, M.M., Buesseler, K., Bathmann, U., Hense, I., Andrews, J., 2002a. Comparison of carbon and opal export rates between summer and spring bloom periods in the region of the Antarctic Polar Front, SE Atlantic. Deep-Sea Research II 49 (18), 3849–3869.

Rutgers van der Loeff, M.M., Meyer, R., Rudels, B., Rachor, E., 2002b. Resuspension and particle transport in the benthic nepheloid layer in and near Fram Strait in relation to faunal abundances and Th-234 depletion. Deep-Sea Research I 49 (11), 1941–1958.

Rutgers van der Loeff, M., Sarin, M.M., Baskaran, M., Benitez-Nelson, C., Buesseler, K.O., Charette, M., Dai, M., Gustafsson, Ö., Masque, P., Morris, P.J., Orlandini, K., Rodriguez y Baena, A., Savoye, N., Schmidt, S., Turnewitsch, R., Vöge, I., Waples, J.T., 2006. A review of present techniques and methodological advances in analyzing ^{234}Th in aquatic systems. Marine Chemistry 100, 190–212.

Sarthou, G., Vincent, D., Christaki, U., Obernosterer, I., Timmermans, K.R., Brussaard, C.P.D., 2008. The fate of biogenic iron during a phytoplankton bloom induced by natural fertilization: impact of

copepod grazing. Deep-Sea Research II, this issue [doi:10.1016/j.dsr2.2007.12.033].

Savoye, N., Buesseler, K.O., Cardinal, D., Dehairs, F., 2004. ^{234}Th deficit and excess in the Southern Ocean during spring 2001: particle export and remineralization. Geophysical Research Letters 31 (12), L12301.

Savoye, N., Benitez-Nelson, C., Burd, A.B., Cochran, J.K., Charette, M., Buesseler, K.O., Jackson, G.A., Roy-Barman, M., Schmidt, S., Elskens, M., 2006. ^{234}Th sorption and export models in the water column: a review. Marine Chemistry 100, 234–249.

Shimmield, G.B., Ritchie, G.D., Fileman, T.W., 1995. The impact of marginal ice-zone processes on the distribution of Pb-210, Po-210 and Th-234 and implications for new production in the Bellingshausen Sea, Antarctica. Deep-Sea Research II 42 (4/5), 1313–1335.

Smetacek, V., Assmy, P., Henjes, J., 2004. The role of grazing in structuring Southern Ocean pelagic ecosystems and biogeochemical cycles. Antarctic Science 16 (4), 541–558.

Sterner, R.W., Elser, J.J., 2002. Ecological Stoichiometry: The Biology of Elements from Molecules to the Biosphere. Princeton University Press.

Takahashi, T., Sutherland, S.C., Sweeney, C., Poisson, A., Metzl, N., Tilbrook, B., Bates, N., Wanninkhof, R., Feely, R.A., Sabine, C., Olafsson, J., Nojiri, Y., 2002. Global sea–air CO_2 flux based on climatological surface ocean pCO2 and seasonal biological and temperature effect. Deep-Sea Research II 49, 1601–1622.

Trull, T.W., Armand, L., 2001. Insights into Southern Ocean carbon export from the δ^{13}C of particles and dissolved inorganic carbon during the SOIREE iron release experiment. Deep-Sea Research II 48, 2655–2680.

Trull, T., Davies, D., Casciotti, K., 2008. Insights into nutrient assimilation and export in naturally iron-fertilized waters of the Southern Ocean from nitrogen, carbon and oxygen isotopes. Deep-Sea Research II, this issue [doi:10.1016/j.dsr2.2007.12.035].

Usbeck, R., Rutgers van der Loeff, M., Hoppema, M., Schlitzer, R., 2002. Shallow remineralization in the Weddell Gyre. Geochemistry Geophysics Geosystems 3 (1), 1008.

Vaillancourt, R.D., Marra, J., Barber, R.T., Smith Jr., W.O., 2003. Primary productivity and in situ quantum yields in the Ross Sea and Pacific sector of the Antarctic Circumpolar Current. Deep-Sea Research II 50 (3/4), 559–578.

Van Beek, P., Bourquin, M., Reyss, J.L., Souhault, M., Charette, M., Jeandel, C., 2008. Radium isotopes to investigate the water mass pathways on the Kerguelen Plateau (Southern Ocean). Deep-Sea Research II, this issue [doi:10.1016/j.dsr2.2007.12.025]

Waples, J.T., Benitez-Nelson, C.R., Savoye, N., Rutgers van der Loeff, M., Baskaran, M., Gustafsson, Ø., 2006. An Introduction to the application and future use of ^{234}Th in aquatic systems. Marine Chemistry 100, 166–189.

Wassmann, P., 1998. Retention versus export food chains: processes controlling sinking loss from marine pelagic systems. Hydrobiologia 363, 29–57.